

Noise Analysis, Calculation and Reduction of External Rotor Permanent Magnet Synchronous Motor

Shuguang Zuo, Fu Lin, and Xudong Wu

Abstract—A detailed analysis of electromagnetic noise in external rotor permanent magnet synchronous motor (PMSM) is presented in this paper. Firstly, the spatial distribution and frequency characteristics of electromagnetic force acting on surface of permanent magnet are discussed. Then, calculation models for electromagnetic force, structural vibration and acoustic radiation are developed to predict noise by taking an external rotor in-wheel motor (IWM) as example. The uneven distribution of electromagnetic force on the surface of permanent magnet is taken into account by means of loading nodal force into structural model which is verified by modal test. Through the mode superposition method the vibration on the surface of outer rotor is calculated and the acoustic boundary element method (BEM) is used to predict the acoustic radiation. Noise test is conducted to validate the simulated noise. It is shown in both simulation results and noise test that the electromagnetic force due to slotting effects contributes the most remarkable component to the overall noise. Finally, slot opening width is optimized to reduce the amplitude of magnetic force close to resonance frequencies and the overall sound pressure level decreases by 6 dB(A) after optimization.

Index Terms—Permanent magnet synchronous motor, external rotor, noise prediction, nodal force, slotting effects, noise optimization.

I. INTRODUCTION

Recent years have witnessed a broad application of fractional slot concentrated winding (FSCW) due to its several advantages such as high power/torque density, high efficiency, low cogging torque, better performance of field weakening operation and fault tolerance [1]. However, compared to the integral slot motor, the spatial harmonic order of electromagnetic force in FSCW motor is lower and the noise problem becomes more significant [2]. Especially in the field requiring low noise, the noise level is an important index to assess the performance of PMSM.

Usually for small and medium-sized motor, electromagnetic noise is the major source of the overall noise and it results from the electromagnetic force acting on the surface of stator and rotor. The spatial distribution and frequency characteristics of

electromagnetic force acting on the surface of stator are widely discussed in [3] [4], and different slot/pole combinations and winding layers are considered. It is proposed in [5] that machines having asymmetrical winding distribution may yield unbalanced magnetic pull and will increase noise level. For PMSM with external stator, electromagnetic force acting on stator surface has been thoroughly studied. However, for PMSM with external rotor, the most noise radiates from the rotor and the electromagnetic noise mainly results from the electromagnetic force acting on the surface of permanent magnet. In [6] spatial and specifically frequency harmonic ordinal numbers of radial force are discussed in external rotor PMSM with non-overlapping windings. The shapes of permanent magnet and teeth are optimized to reduce the force fluctuation induced by stator slotting. However, the force features in external rotor PMSM with different slot/pole combinations are still needed to be analyzed and some nonideal factors such as current harmonics should be taken into account.

Analytical and numerical methods are both employed to calculate the vibration and noise of PMSM. A 2D analytical vibration model is established in [7]. By using this model a quick calculation of vibration and noise is achieved, but the effects of end belts on the structural intrinsic property is neglected. These effects could be quite enormous according to the research in [8]. In [9] structural intrinsic property is obtained by mechanical impulse response instead of modal test, and then vibration is calculated by loading the force into the center of teeth surface. A multi-physics NVH model for SRM is presented in [10], and noise peaks are validated by noise test. However, in [9] and [10] the uneven distribution of electromagnetic force along a tooth surface is equivalent to a concentrated force acting on the center of the surface. Similar simplifications can also be found in [8], [11], [12], which may induce extra calculation error. In [13] electromagnetic impulse response is used to obtain the structural intrinsic property, and with the vibration information of some points, modal expansion method is used to predict the whole vibration of stator. The calculated vibration of other points agrees well with vibration test. However, in this calculation procedure a vibration test should be conducted in advance to get the vibration information of some points.

For vibration and noise reduction, optimization of electromagnetic force and increase of structural stiffness are both used. But the latter method requires a relatively high cost. The most widely used method to reduce the vibration and noise

Manuscript received September 16, 2014; revised January 20, 2015 and March 4, 2015; accepted April 5, 2015.

Copyright (c) 2015 IEEE. Personal use of this material is permitted. However, permission to use this material for any other purposes must be obtained from the IEEE by sending a request to pubs-permissions@ieee.org.

The authors are with Clean Energy Automotive Engineering Center, Tongji University, No.4800, Cao'an Road, Jiading District, Shanghai, China. (e-mail: sgzuo@tongji.edu.cn; linfu_911@163.com; wuxudong@tongji.edu.cn).

is to eliminate the electromagnetic force close to the modal frequency. In [14] the electromagnetic force produced by current harmonics is adapted to be apart from the resonance region by optimal choice of the carrier frequency and vibration is reduced by 35%. A skewed stator is used in [15] and [16] to reduce the amplitude of electromagnetic force close to modal frequencies, and in [16] the calculation method of optimal skewed angle is proposed. The minimization of vibration and noise is realized in [17] by forming optimal notches on the rotor pole face. In this method the electromagnetic excitation having harmonic order of $12n$ which contributes the most remarkable component to the overall noise is reduced by elimination of 3rd harmonic of the air-gap field. However, in PMSM with external rotor, the optimization method for noise reduction is different from PMSM with external stator due to the change of excitation features.

In this research, the spatial distribution and frequency characteristic of electromagnetic force acting on surface of permanent magnet are firstly derived and the effects of slot/pole combinations are considered. Then models for electromagnetic force, structural vibration and acoustic radiation of an IWM for electric vehicles are developed. Electromagnetic force under no load and under load is analyzed and the uneven distribution of electromagnetic force is considered when the force is loaded to the surface of permanent magnet. The mode superposition method is used to calculate the vibration of external rotor and the acoustic noise of IWM is calculated by BEM. Finally, a practical method by optimization of slot opening width is proposed to reduce the noise level of PMSM with external rotor.

II. ELECTROMAGNETIC FORCE ANALYSIS

In a PMSM the air-gap field is composed of permanent magnet field and armature reaction field, and the effect of slotting on air-gap field can be analyzed by relative permeance function λ_a . The resultant radial flux density B_{rs} in air-gap is expressed as

$$B_{rs} = (B_{r_mag} + B_{r_arm})\lambda_a \quad (1)$$

where B_{r_mag} and B_{r_arm} are the slotless radial permanent magnet field and slotless radial armature reaction field, respectively. λ_a is the real part of relative permeance.

Neglecting the tangential flux density component [7], radial force density can be evaluated by Maxwell's stress method. Thus,

$$f_r \approx \frac{B_{rs}^2}{2\mu_0} \quad (2)$$

For external rotor PMSM, the outside rotor is the main radiator of electromagnetic noise. So we are concerned about the electromagnetic force acting on the inner surface of permanent magnet. Thus it can be assumed that the outside rotor is fixed and the stator rotates in the opposite direction with an angular velocity ω_r . In rotor coordinates B_{r_mag} , B_{r_arm} and λ_a can be written as

$$B_{r_mag} = \sum_n B_{mn} \cos(np\theta) \quad (3)$$

$$B_{r_arm} = \sum_v B_{av} \sin[vp(\theta + \omega_r t) + s_v p \omega_r t] \quad (4)$$

$$\lambda_a = \lambda_0 + \sum_\mu \lambda_{a\mu} \cos[\mu Q_s(\theta + \omega_r t)] \quad (5)$$

here, θ is the spatial mechanical angle, t is the time, p is the number of pole pairs and Q_s is the number of slots. s_v denotes the rotation direction of v^{th} harmonic of armature reaction field, being -1 for forward rotating and 1 for back rotating.

For PMSM with different slot pole combinations and double layer windings, the value of $(s_v + v)p$ is [19]

$$(s_v + v)p = 3kN_{ps}, (k = 1, 2, 3, \dots) \quad (6)$$

here, $N_{ps} = \text{GCD}(2p, Q_s)$, is the greatest common divisor of the numbers of poles and slots. Radial force density can be obtained by substituting (3), (4) and (5) into (2). It can be written as

$$\begin{aligned} f_r &= \frac{1}{2\mu_0} \left[\sum_n B_{mn} \cos(np\theta) + \sum_v B_{av} \sin(vp\theta + 3kN_{ps}\omega_r t) \right]^2 \\ &\times \left[\lambda_0 + \sum_\mu \lambda_{a\mu} \cos(\mu Q_s \theta + \mu Q_s \omega_r t) \right]^2 \\ &= \frac{1}{4\mu_0} \left\{ \sum_{n_1 n_2} B_{mn_1} B_{mn_2} [\cos(n_1 + n_2)p\theta + \cos(n_1 - n_2)p\theta] \right. \\ &\quad + 2 \sum_n \sum_v B_{mn} B_{av} \left\{ \begin{aligned} &\sin[(n + v)p\theta + 3kN_{ps}\omega_r t] \\ &-\sin[(n - v)p\theta - 3kN_{ps}\omega_r t] \end{aligned} \right\} \\ &\quad + \sum_{v_1 v_2} B_{av_1} B_{av_2} \left\{ \begin{aligned} &\cos[(v_1 - v_2)p\theta + 3(k_1 - k_2)N_{ps}\omega_r t] \\ &-\cos[(v_1 + v_2)p\theta + 3(k_1 + k_2)N_{ps}\omega_r t] \end{aligned} \right\} \Big\} \\ &\times \left\{ \lambda_0^2 + 2\lambda_0 \sum_\mu \lambda_{a\mu} \cos(\mu Q_s \theta + \mu Q_s \omega_r t) \right. \\ &\quad \left. + \frac{1}{2} \sum_{\mu_1 \mu_2} \lambda_{a\mu_1} \lambda_{a\mu_2} \left\{ \begin{aligned} &\cos[(\mu_1 + \mu_2)Q_s \theta + (\mu_1 + \mu_2)Q_s \omega_r t] \\ &+ \cos[(\mu_1 - \mu_2)Q_s \theta + (\mu_1 - \mu_2)Q_s \omega_r t] \end{aligned} \right\} \right\} \Big\} \quad (7) \end{aligned}$$

According to the rule of polynomial multiplication, (7) results in 9 terms, which can be divided into 6 classes according to the source. The amplitude, spatial order and frequency of these 6 sources of force are derived by product to sum formula of trigonometric function, as shown in Table I.

TABLE I
SOURCE, AMPLITUDE, SPATIAL ORDER AND FREQUENCY OF
RADIAL FORCE DENSITY

Source	Amplitude	Spatial order	Frequency
Permanent magnet field	$\frac{1}{4\mu_0} \lambda_0^2 B_{mn_1} B_{mn_2}$	$(n_1 \pm n_2)p$	0
Armature reaction field	$\frac{1}{4\mu_0} \lambda_0^2 B_{av_1} B_{av_2}$	$(v_1 \pm v_2)p$	$3(k_1 \pm k_2)N_{ps}f_r$
Interaction of permanent magnet field	$\frac{1}{2\mu_0} \lambda_0^2 B_{mn} B_{av}$	$(v \pm n)p$	$3kN_{ps}f_r$

and armature reaction field			
Interaction of permanent magnet field and stator slotting	$\frac{1}{4\mu_0}\lambda_0\lambda_{a\mu}B_{mn1}B_{mn2}$	$(n_1\pm n_2)p\pm\mu Q_s$	μQ_{sf_r}
	$\frac{1}{16\mu_0}\lambda_{a\mu_1}\lambda_{a\mu_2}B_{mn1}B_{mn2}$	$(n_1\pm n_2)p\pm(\mu_1\pm\mu_2)Q_s$	$(\mu_1\pm\mu_2)Q_{sf_r}$
Interaction of armature reaction field and stator slotting	$\frac{1}{4\mu_0}\lambda_0\lambda_{a\mu}B_{av1}B_{av2}$	$(v_1\pm v_2)p\pm\mu Q_s$	$3(k_1\pm k_2)N_{ps}f_r\pm\mu Q_{sf_r}$
	$\frac{1}{16\mu_0}\lambda_{a\mu_1}\lambda_{a\mu_2}B_{av1}B_{av2}$	$(v_1\pm v_2)p\pm(\mu_1\pm\mu_2)Q_s$	$3(k_1\pm k_2)N_{ps}f_r\pm(\mu_1\pm\mu_2)Q_{sf_r}$
Interaction of permanent magnet field, armature reaction field and stator slotting	$\frac{1}{2\mu_0}\lambda_0\lambda_{a\mu}B_{mn1}B_{av}$	$(v\pm n)p\pm\mu Q_s$	$3kN_{ps}f_r\pm\mu Q_{sf_r}$
	$\frac{1}{8\mu_0}\lambda_{a\mu_1}\lambda_{a\mu_2}B_{mn1}B_{av}$	$(v\pm n)p\pm(\mu_1\pm\mu_2)Q_s$	$3kN_{ps}f_r\pm(\mu_1\pm\mu_2)Q_{sf_r}$

It can be seen from Table I that the frequency of electromagnetic force under no load is equal to μQ_{sf_r} which comes from the interaction of permanent magnet field and stator slotting. The frequency of electromagnetic force is equal to $3kN_{ps}f_r$ under load. It is well known that the frequency of electromagnetic force acting on the surface of stator is equal to $2kp f_r$ when the machine is excited by sinusoidal current. Thus, the frequency characteristics of noise radiated by external rotor PMSM is different from that of external stator PMSM. However, the spatial characteristics in these two kinds of PMSM are the same. For PMSM with double layer windings, the spatial order is equal to the integral multiple of N_{ps} .

An external rotor IWM for electrical vehicles (as shown in Fig. 1) is taken for example to analyze the electromagnetic force acting on the inner surface of permanent magnet. The main parameters of IWM are listed in Table II. In order to compare the simulated noise with experimental noise which is tested under 40Nm load torque with a rotation speed of 500rpm, the electromagnetic force is also computed under the same load torque and rotation speed. The excited current profile is obtained by test and its time history and frequency spectrum are shown in Fig. 2. The rated speed of this IWM is 290 rpm and the motor is used in low-speed applications. When it is overloaded and works in high speed, the amplitudes of current harmonics get higher. The electromagnetic force under no load is also calculated.

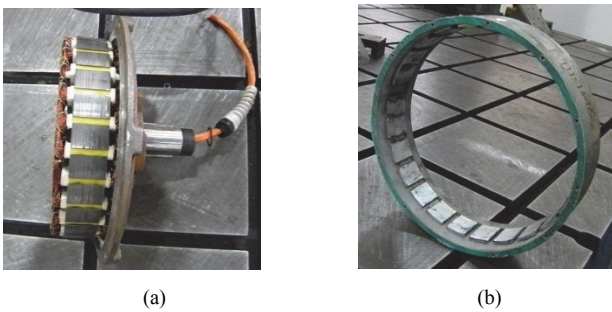


Fig. 1 In-wheel motor. (a) stator. (b) rotor.

TABLE II MAIN PARAMETERS OF IN-WHEEL MOTOR	
Items	Value(Unit)
Number of poles/slots	24/27
Outer radius of rotor	137.25mm
Thickness of rotor-back iron	7.5mm
Length of air-gap	1mm
Thickness of permanent magnet(PM)	3.5mm
Remnant flux density of PM	1.2T
Stack length of stator	35mm
Number of turns per coil	13
Slot opening width	6mm
Pole-arc coefficient	0.9

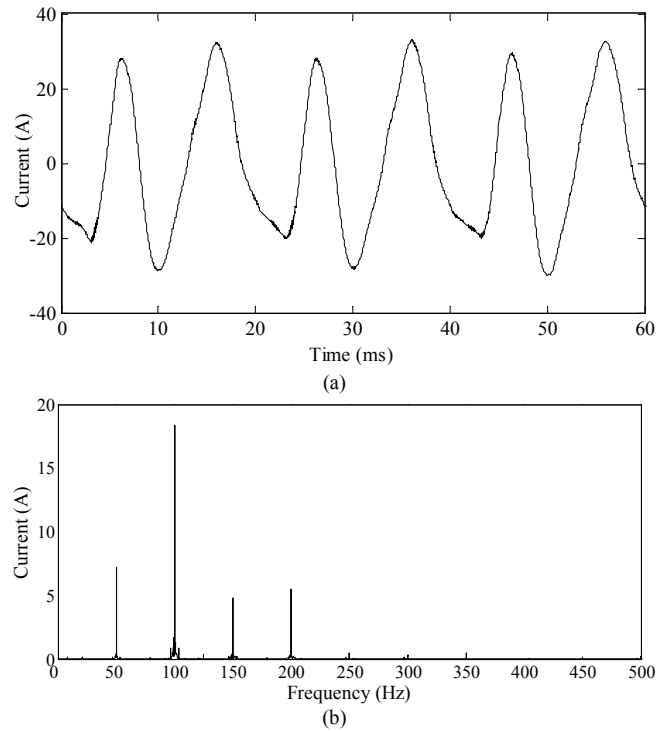


Fig. 2 Tested current under 40 Nm load torque with a rotation speed of 500rpm. (a) time history. (b) frequency spectrum.

For this IWM with 24 poles and 27 slots, N_{ps} is equal to 3, which means it can be considered that the IWM is composed of 3 8-pole/9-slot motors for force analysis. Thus, a 1/3 2D model for force calculation of IWM is built. Fig. 3 shows the distribution of electromagnetic force on the surface of permanent magnet under no load and under load. The uneven distribution along the magnet surface under load becomes more severe due to the effect of armature reaction field which makes airgap field fluctuate more widely.

Fig. 4 shows the frequency spectrum of radial force density in the middle of a permanent magnet surface under no load and under load. The frequency of electromagnetic force is equal to $\mu Q_{sf_r}=27\times 500/60\times\mu=225\mu$ ($\mu=1, 2, 3, \dots$) under no load according to Table I. However, when the IWM is excited by current whose frequency spectrum is shown in Fig. 2, electromagnetic force harmonics become richer, especially in low frequencies. This part of force harmonics comes from the interaction of fundamental permanent magnet field and

armature reaction field produced by current harmonics. Due to the low frequency of fundamental permanent magnet field and current harmonics, this part of force concentrates in low frequency band. So in high frequency band, the force under no load and under load are almost same because this part of force comes from the interaction of magnet field and stator slotting, as shown in Fig. 4. The rich force harmonics in low frequency band may increase the likelihood of resonance and exacerbate the vibration and noise.

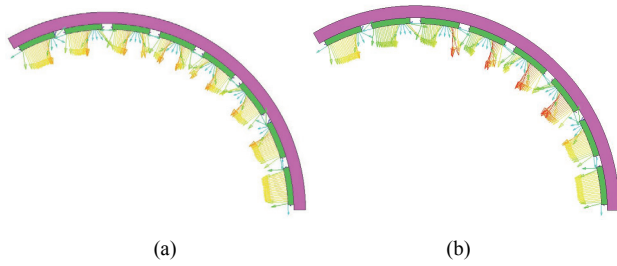


Fig. 3 Distribution of electromagnetic force on the surface of permanent magnet. (a) under no load. (b) under load.

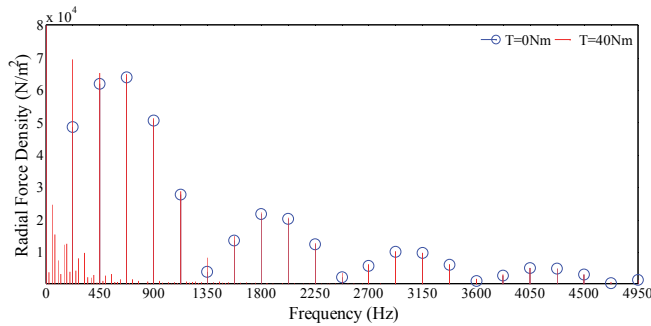


Fig. 4 Spectrum of electromagnetic force under no load and under load

III. CALCULATION OF VIBRATION AND NOISE

A multi-physics model is established to calculate the vibration and noise of IWM. Firstly, a 1/3 2D electromagnetic finite element model is built to calculate the nodal force on the surface of permanent magnet. Nodal force in 3D full model is obtained according to the periodicity of IWM and assuming that the electromagnetic force distributes uniformly in the axial direction. Then, 3D structural model of IWM is built and modal test is employed to validate the model. The nodal force is loaded from electromagnetic model to structural model by force interpolation. In this way the uneven distribution of electromagnetic force is taken into account. Finally, modal superposition method is used to calculate the vibration and BEM is adopted to calculate the acoustic noise. The general procedure of noise calculation of IWM is shown in Fig. 5.

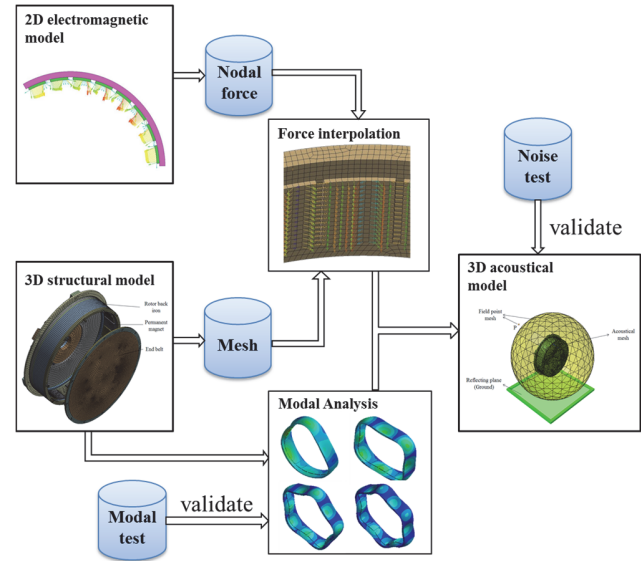


Fig. 5 Noise calculation procedure of IWM

A. Modal Analysis of IWM

As shown in Fig. 6, a structural finite element model of IWM composed of end belt, permanent magnet and rotor back iron is built. In order to validate the model, modal test is conducted. In the test, IWM was suspended by soft nylon ropes to approximate to free support condition. 18 acceleration sensors were distributed uniformly along the circumference direction on the surface of rotor, as shown in Fig. 7. Modal shape and frequency from simulation and test are compared in Table III. End belt is hidden in order to observe the modal shape more clearly. It is shown that the relative errors between the calculated and the measured modal frequencies are all below 2%. This comparison demonstrates the accuracy of the structural finite element model.

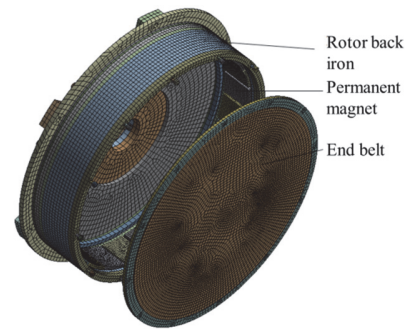
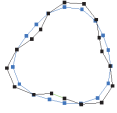
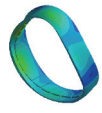
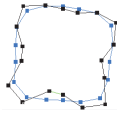
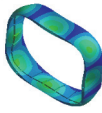
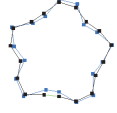





Fig. 6 Structural finite element model of IWM



Fig. 7 Modal test of IWM

TABLE III
COPARISON OF MODAL SHAPE AND FREQUENCY FROM
SIMULATION AND TEST

Mode order	Measured mode shape and frequency	Calculated mode shape and frequency	Relative error
3	 3856.7 Hz	 3848.5 Hz	0.21%
4	 4804.1 Hz	 4819.5 Hz	0.32%
5	 5840.2 Hz	 5782.9 Hz	0.98%
6	 7044.1 Hz	 6936.0 Hz	1.53%

B. Loading of Nodal Force

The electromagnetic force acting on the surface of stator and rotor is a spatial rotating force wave. Thus, it's a tough work to load this kind of force into the structural model for vibration calculation. Many researchers simplify the loading procedure and the uneven distribution of electromagnetic force along a tooth surface is equivalent to a concentrated force acting on the center of the surface. However, this simplification may induce a considerable error in the noise calculation of external rotor PMSM.

Fig. 8 shows the spatial and temporal distribution of radial electromagnetic force under no load and under load. After the force in a pole pitch is integrated, the uneven distribution characteristic is changed and the fluctuation of the force decreases, as shown in Fig. 9. Compare the force under no load for example, Fig. 8 tells us that the amplitude of the force in a point of a permanent magnet surface can change about 50%. However, a small change is shown after integration in Fig. 9.

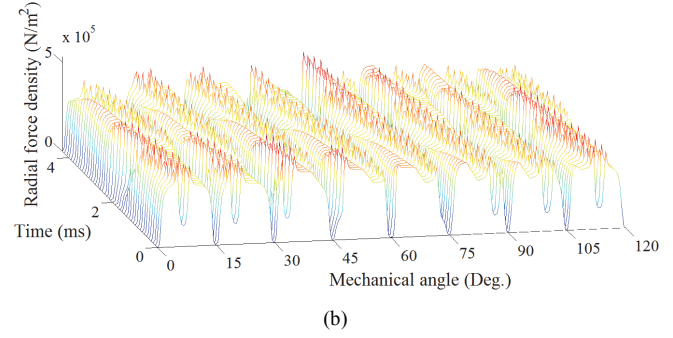
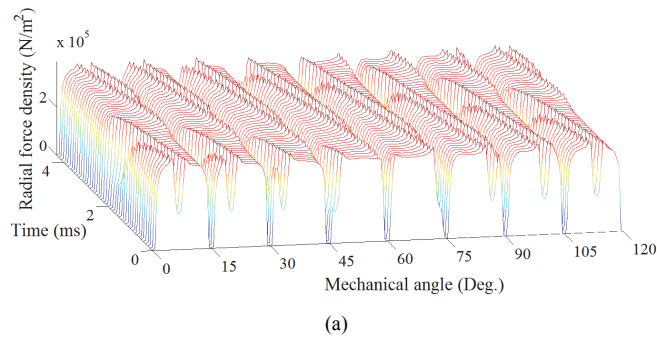


Fig. 8 Spatial and temporal distribution of electromagnetic force. (a) under no load. (b) under load

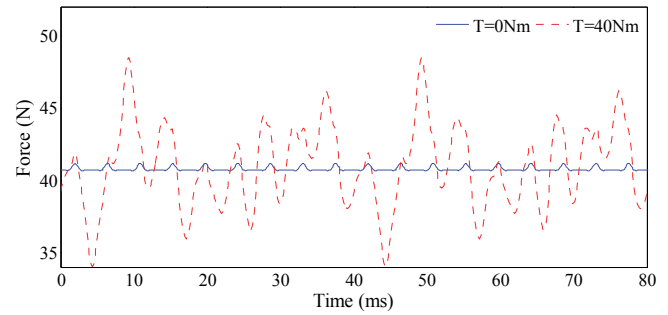


Fig. 9 The equivalent concentrated force by integrated the electromagnetic force in a pole pitch.

In order to take the uneven distribution characteristics into account, electromagnetic force is loaded into the structural model through nodal force. Firstly, a 1/3 2D electromagnetic model is built to calculate the nodal force acting on the surface of permanent magnet. And nodal force in 3D space is obtained according to the periodicity of IWM and assuming that the electromagnetic force distributes uniformly in the axial direction. Force interpolation is used to apply the electromagnetic nodal force to structural nodes. Fig. 10 shows the nodal force in the structural model.

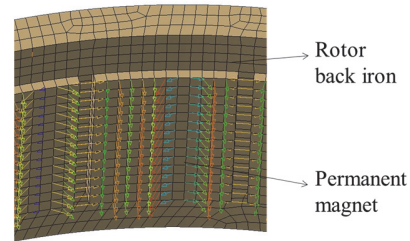


Fig. 10 Nodal force in the structural model

C. Calculation of Vibration

Based on the accurate structural model and force loading, mode superposition method is used to calculate the vibration of IWM. The calculation equations is expressed as

$$[M] \sum_{i=1}^N \{\Phi_i\} \ddot{x}_i + [C] \sum_{i=1}^N \{\Phi_i\} \dot{x}_i + [K] \sum_{i=1}^N \{\Phi_i\} x_i = \{F\} \quad (8)$$

Here, x_i is nodal displacement in modal coordinates, $\{\Phi_i\}$ is the modal shape of mode i , $\{F\}$ is the electromagnetic nodal force varying in time, N is the number of modes to be summed, and

$\{M\}$, $\{C\}$ and $\{K\}$ are the mass matrix, the damping matrix, and the stiffness matrix, respectively. $\{M\}$, $\{K\}$, $\{\Phi_i\}$, and $\{F\}$ are calculated numerically and $\{C\}$ is obtained from modal test.

Fig. 11 shows the acceleration spectrum of the center point of the outside end belt under no load and under load. Vibration under load becomes more severe, especially in low frequencies, e.g. between 0 Hz and 450 Hz, which is caused by abundant force harmonics produced by current harmonics, as shown in Fig. 4.

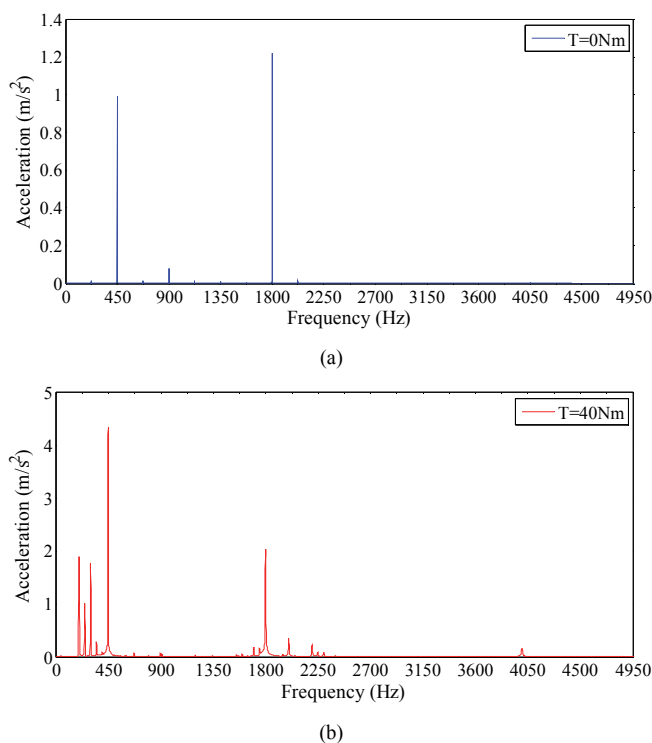


Fig. 11 Acceleration of the center point of the end belt. (a) under no load. (b) under load.

It can be seen in Fig. 11 that two of the largest vibration peaks appear at the frequencies of 450 Hz and 1800 Hz. By using fast Fourier transform (FFT) we can get general vibration of external rotor in these two frequencies, as shown in Fig. 12. IWM has a short axial length and the external rotor is connected to the stator by a single slide bearing through the inside end belt, which leads to less restrictions of outside end belt. Moreover, in order to reduce the weight of IWM, the outside end belt has a thickness of 3.5 mm and is made of aluminum. Though the electromagnetic force act on the inner surface of permanent magnets which are connected to the rotor back iron, the outside end belt exhibits more severe vibration due to its low stiffness.

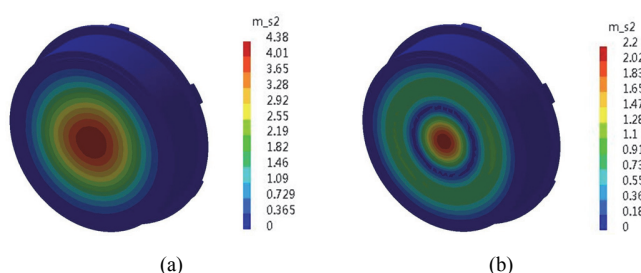


Fig. 12 General vibration of external rotor. (a) 450Hz. (b) 1800Hz

From the modal analysis, we can find the modal shape close to this two vibration peaks, as shown in Fig. 13. Due to the special construction of IWM as the previous analysis, the stiffness of the outside end belt is quite low and the modal frequency of the end belt appears in low frequencies. Moreover, it is shown in Fig. 4 the amplitude of electromagnetic force is higher and force harmonics become more abundant in low frequencies. When this part of force with larger amplitude is close to the local modes of the end belt, resonance happens and the vibration becomes more severe.

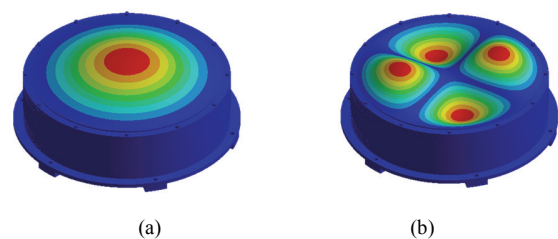


Fig. 13 Modal shape and frequencies of local modes of the outside end belt. (a) 486.7 Hz. (b) 1776.0 Hz.

D. Noise prediction and experimental verification

Based on the vibration calculation result, BEM is used to predict the acoustic noise of IWM. This noise prediction method is different from the conventional FEM. It needs external surface vibration of rotor to serve as acoustic boundary condition and has not to discrete the space between sound source and field point as FEM. So BEM is more efficient than the conventional FEM and used to solve motor radiation noise problems in [10], [13] and [20]. Fig. 14 shows the acoustic boundary element model of IWM which contains the acoustical mesh, field point mesh and reflecting plane simulating the ground. The field point P corresponds to the position of microphone in the noise test.

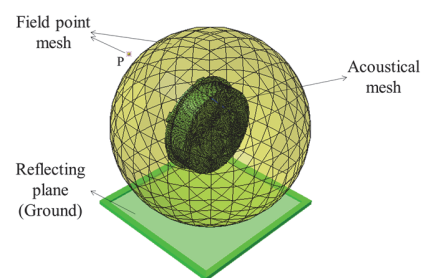


Fig. 14 Acoustical boundary element model of IWM

The noise calculation result of the acoustic boundary element model is compared with the tested noise in the semi-anechoic room, as shown in Fig. 15. The calculated noise peaks can also be found in the test and the noise curve exhibits the same trend in the spectrum with the tested noise. It can be seen in both calculated and tested results the noise peaks mainly concentrate at frequencies of 225μ , which is equal to $\mu Q_s f_r$. Fig. 16 shows the noise spectrum under no load. Due to the abundant electromagnetic force harmonics in low frequencies, the noise spectrum under load shows more harmonics in this frequency

band than the spectrum under no load. However, in high frequencies, the noise spectrum under no load and under load are almost same, which can be explained by the force spectrum shown Fig. 4 in which the force amplitude and harmonics in these two working conditions have little difference in high frequencies.

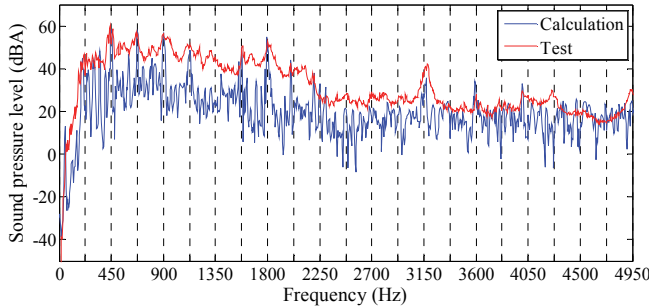


Fig. 15 Validation of the boundary element model by comparing the tested sound pressure level with that calculated by BEM.

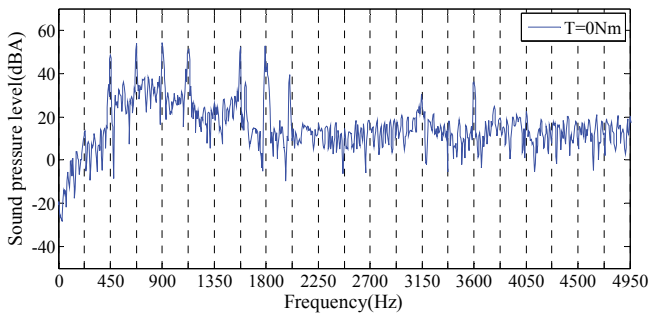


Fig. 16 The noise spectrum under no load with a rotating speed of 500 rpm.

IV. NOISE OPTIMIZATION

It can be concluded from Fig. 4, Fig. 15 and Fig. 16 that the electromagnetic force produced by the interaction of permanent magnet field and stator slotting contributes most to the electromagnetic noise of IWM. The frequency of this part of force is equal to $\mu Q_s f_r$. Moreover, we can find in Table I that the amplitude of this part of force is proportional to λ_{au} which is also related to slot opening width b . Thus, the relationship between the overall noise level and b is discussed in this chapter.

λ_{au} can be obtained either by solving the nonlinear equations in [18] or by finite element analysis (FEA). A finite element method solving λ_{au} is introduced here. The permanent magnet field accounting for slotting effects can be expressed as

$$\begin{cases} B_{rs_mag} = B_{r_mag} \lambda_a + B_{t_mag} \lambda_b \\ B_{ts_mag} = B_{t_mag} \lambda_a - B_{r_mag} \lambda_b \end{cases} \quad (9)$$

Here, B_{t_mag} , B_{rs_mag} and B_{ts_mag} are slotless tangential, slotted radial and slotted tangential permanent magnet field, respectively. λ_b is the imaginary part of relative permeance. B_{r_mag} , B_{t_mag} , B_{rs_mag} and B_{ts_mag} can be obtained by magnetostatic field analysis using 2D FEM. Thus, λ_a is solved by using (9) and λ_{au} is obtained by harmonic analysis of λ_a .

The noise peaks can be found in Fig. 16 at the frequencies of 450 Hz, 675 Hz, 900 Hz, 1125 Hz, 1575 Hz, 1800 Hz and the corresponding values of μ are equal to 2, 3, 4, 5, 7, 8,

respectively. Fig. 17 shows the relationship between the corresponding λ_{au} of these values and the slot opening width b by using FEA. The amplitude of electromagnetic force at frequency of $\mu Q_s f_r$ under no load is related to b in the same trend. It is also seen in Fig. 17 when μ is higher, more values of b can be found in a certain slot opening width range to make λ_{au} zero.

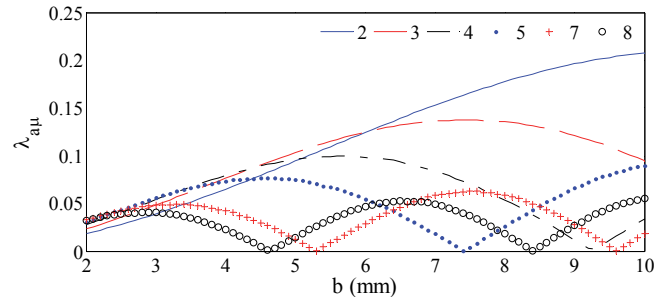


Fig. 17 The relationship between λ_{au} and b

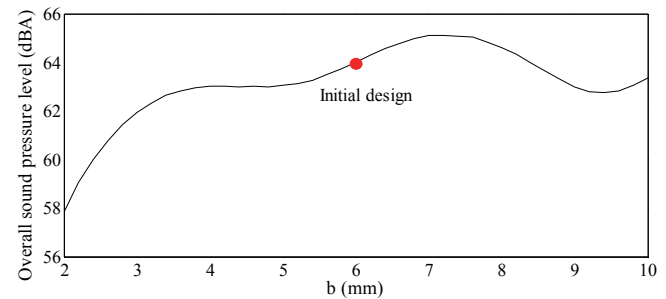


Fig. 18 The relationship between overall sound pressure level and b

BEM is used to analyze the relationship between the overall sound pressure level (SPL) of IWM and the slot opening width b , as shown in Fig. 18. In the initial design whose b is equal to 6mm, the overall SPL reaches 64 dB(A). When b is reduced to 2mm, the overall SPL decreases to 58 dB(A). In Fig. 19, the electromagnetic force, vibration of the center point of the end belt and the noise spectrum under no load are compared under these two slot opening widths. It is shown in Fig. 19 (a) amplitudes of forces close to the modes of the end belt shown in Fig. 13 decreases sharply. Hence, the amplitudes of the vibration acceleration at frequencies of 450 Hz and 1800 Hz which contributes most to the general vibration decrease 89.6% and 73.3%, respectively. The noise amplitudes at the corresponding frequencies have also 22 dB(A) and 31 dB(A) drop, respectively. Moreover, except for the slight increase of noise harmonic amplitudes at the frequencies of 1350, 1575, 2025 and 2475 Hz, the amplitude of other harmonics also decreases at different levels. Thus, it is an effective method to reduce acoustic noise of external rotor PMSM by using slot opening width optimization. This method is also practical because it does not require big changes in motor structure.

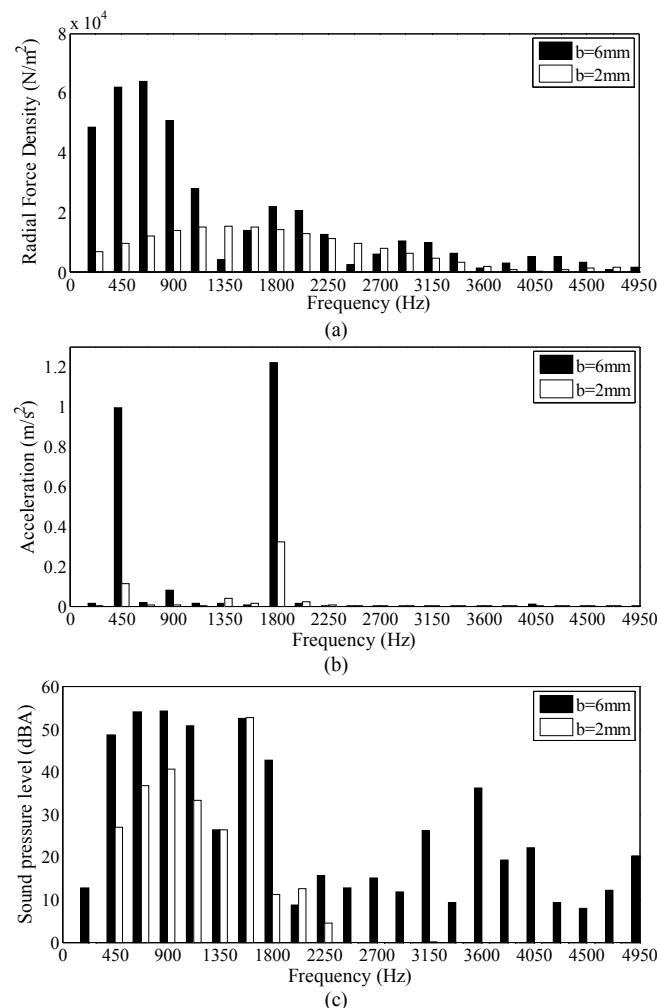


Fig. 19 Electromagnetic force, vibration acceleration and noise spectrum comparison under different slot opening widths. (a) electromagnetic force. (b) vibration acceleration. (c) noise

V. CONCLUSION

The spatial distribution and frequency characteristics of external rotor PMSM with different slot-pole combinations are discussed in this paper. The spatial harmonics in the external rotor and external stator PMSM are the same. For PMSM with external rotor, the frequency of the electromagnetic force is equal to $\mu Q_s f_r$ and $3kN_{ps} f_r$ under no load and under load, respectively. This frequency characteristic is different from that in external stator PMSM in which the frequency of the electromagnetic force is equal to $2kp f_r$.

An IWM for electric vehicles is used to present the calculation procedure of the acoustic noise of external rotor PMSM. Three calculation models for electromagnetic force, structural vibration and noise radiation are proposed to predict the IWM noise. The uneven distribution of electromagnetic force and the tangential force are taken into account by introducing nodal force loading and force interpolation. The calculated noise is validated by the noise test. And it is shown in both calculated and tested results that the electromagnetic force at the frequency equal to $\mu Q_s f_r$ produced by the interaction

of permanent magnet field and stator slotting contributes the most remarkable component to the overall noise.

The relationship of the electromagnetic force and slot opening width is discussed to reduce noise of IWM. When the slot opening width is reduced from 6mm to 2mm, the overall SPL decreases 6 dB(A). This effective method for noise reduction of external rotor PMSM by optimization of the slot opening width is also practical because it requires small changes in motor structure.

ACKNOWLEDGEMENT

This work was supported in part by a Grant (Project 51375343) from the National Natural Science Foundation of China, in part by a Grant (Project 2012YQ150256) from the National Major Scientific Instrument Equipment Project of China and in part by a Grant (Project 51305303) from the National Natural Science Foundation of China.

REFERENCES

- [1] M. EL-Refaie, "Fractional-Slot Concentrated-Windings Synchronous Permanent Magnet Machines: Opportunities and Challenges," *IEEE Trans. Ind. Electron.*, vol. 57, no. 1, pp. 107-121, Jan. 2010.
- [2] F. Magnussen and H. Lendenmann, "Parasitic Effects in PM Machines With Concentrated Windings," *IEEE Trans. Ind. Appl.*, vol. 43, no. 5, pp. 1223-1232, Sept./Oct. 2007.
- [3] Z. Q. Zhu, Z. P. Xia, L. J. Wu, and G. W. Jewell, "Influence of slot and pole number combination on radial force and vibration modes in fractional slot PM brushless machines having single- and double-layer windings," in *Energy Conversion Congress and Exposition*, 2009, pp. 3443-3450.
- [4] Z. Q. Zhu, Z. P. Xia, L. J. Wu, and G. W. Jewell, "Analytical Modeling and Finite-Element Computation of Radial Vibration Force in Fractional-Slot Permanent-Magnet Brushless Machines," *IEEE Trans. Ind. Appl.*, vol. 46, no. 5, pp. 1908-1918, Sept./Oct. 2010.
- [5] Z. Q. Zhu, M. L. M. Jamil, and L. J. Wu, "Influence of slot and pole number combinations on unbalanced magnetic force in permanent magnet machines," in *Energy Conversion Congress and Exposition*, 2011, pp. 3291-3298.
- [6] J. Krottsch and B. Piepenbreier, "Radial Forces in External Rotor Permanent Magnet Synchronous Motors With Non-Overlapping Windings," *IEEE Trans. Ind. Electron.*, vol. 59, no. 5, pp. 2267-2276, May. 2012.
- [7] Islam and I. Husain, "Analytical Model for Predicting Noise and Vibration in Permanent-Magnet Synchronous Motors," *IEEE Trans. Ind. Appl.*, vol. 46, no. 6, pp. 2346-2354, Nov./Dec. 2010.
- [8] D. Torregrossa, F. Peyraut, B. Fahimi, J. M'Boua, and A. Miraoui, "Multiphysics Finite-Element Modeling for Vibration and Acoustic Analysis of Permanent Magnet Synchronous Machine," *IEEE Trans. Energy Convers.*, vol. 26, no. 2, pp. 490-500, Jun. 2011.
- [9] D. Torregrossa, B. Fahimi, F. Peyraut, and A. Miraoui, "Fast Computation of Electromagnetic Vibrations in Electrical Machines via Field Reconstruction Method and Knowledge of Mechanical Impulse Response," *IEEE Trans. Ind. Electron.*, vol. 59, no. 2, pp. 839-847, Feb. 2012.
- [10] F. L. M. Dos Santos, J. Anthonis, F. Naclerio, J. J. C. Gyselinck, H. Van der Auweraer, and L. C. S. Goes, "Multiphysics NVH Modeling: Simulation of a Switched Reluctance Motor for an Electric Vehicle," *IEEE Trans. Ind. Electron.*, vol. 61, no. 1, pp. 469-476, Jan. 2014.
- [11] D. Y. Kim, G. H. Jang and J. K. Nam, "Magnetically Induced Vibrations in an IPM Motor Due to Distorted Magnetic Forces Arising From Flux Weakening Control," *IEEE Trans. Magn.*, vol. 49, no. 7, pp. 3929-3932, Jul. 2013.
- [12] M. Islam, R. Islam and T. Sebastian, "Noise and Vibration Characteristics of Permanent Magnet Synchronous Motors Using Electromagnetic and Structural Analyses," *IEEE Trans. Ind. Appl.*, vol. 50, no. 5, pp. 3214-3222, Oct. 2014.
- [13] L. Chenjie and B. Fahimi, "Prediction of Acoustic Noise in Switched Reluctance Motor Drives," *IEEE Trans. Energy Convers.*, vol. 29, no. 1,

- pp. 250-258, Mar. 2014.
- [14] D. Torregrossa, D. Paire, F. Peyraut, B. Fahimi, and A. Miraoui, "Active Mitigation of Electromagnetic Vibration Radiated by PMSM in Fractional-Horsepower Drives by Optimal Choice of the Carrier Frequency," *IEEE Trans. Ind. Electron.*, vol. 59, no. 3, pp. 1346-1354, Mar. 2012.
 - [15] K. Do-Jin, J. Jae-Woo, H. Jung-Pyo, K. Kwang-Jin, and P. Chul-Jun, "A Study on the Design Process of Noise Reduction in Induction Motors," *IEEE Trans. Magn.*, vol. 48, no. 11, pp. 4638-4641, Nov. 2012.
 - [16] A. Cassat, C. Espanet, R. Coleman, L. Burdet, E. Leleu, D. Torregrossa, J. M'Boua, and A. Miraoui, "A Practical Solution to Mitigate Vibrations in Industrial PM Motors Having Concentric Windings," *IEEE Trans. Ind. Appl.*, vol. 48, no. 5, pp. 1526-1538, Sept./Oct. 2012.
 - [17] H. Jin, R. Jin-Wook, K. Byeong-Woo, and K. Gyu-Hong, "Vibration Reduction of IPM-Type BLDC Motor Using Negative Third Harmonic Elimination Method of Air-Gap Flux Density," *IEEE Trans. Ind. Appl.*, vol. 47, no. 3, pp. 1300-1309, May/Jun. 2011.
 - [18] D. Zarko, D. Ban and T. A. Lipo, "Analytical calculation of magnetic field distribution in the slotted air gap of a surface permanent-magnet motor using complex relative air-gap permeance," *IEEE Trans. Magn.*, vol. 42, no. 7, pp. 1828-1837, Jul. 2006.
 - [19] P. Salminen, M. Niemela, J. Pyhonen, and J. Mantere, "Performance analysis of fractional slot wound PM-motors for low speed applications," in *Industry Applications Conference, 2004. 39th IAS Annual Meeting*, 2004, pp. 1032-1037.
 - [20] S. Park, W. Kim and S. Kim, "A Numerical Prediction Model for Vibration and Noise of Axial Flux Motors," *IEEE Trans. Ind. Electron.*, vol. 61, no. 10, pp. 5757-5762, Oct. 2014.

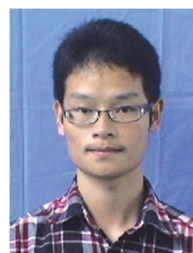


Shuguang Zuo was born in Yuanjiang city, Hunan, China, in 1968. He received the B.S.E. degree in mechanical design, Hunan Agricultural University, Changsha, Hunan, China, in 1990. He received the M.S. degree in 1993 and the PhD degree in 1996 in automotive engineering, Jilin University, Changchun, Jilin, China.

From 1996 to 1998, He was a Postdoctoral Researcher with Aviation and Aerospace Technology Postdoctoral Research Station, Nanjing Aeronautics and Astronautics University, Nanjing, Jiangsu, China.

He is currently Professor of College of Automotive Engineering, Tongji University, Shanghai, China. His research interests include vehicle system dynamics and control, vehicle vibration and noise control, and vibration and noise of electrical machines.

Prof. Zuo is member of American Society of Automotive Engineers, expert of National "863 Program" Expert Database of China, evaluation expert of Shanghai Science and Technology Committee, and peer review expert of National Natural Science Foundation. Prof. Zuo obtained the 11th Shu Guang Scholar Award of Shanghai.



Fu Lin was born in Sanming city, Fujian, China, in 1989. He received the B.S.E. degree in automotive engineering, Tongji University, Shanghai, China, in 2013. He is currently pursuing the PhD degree in automotive engineering at Tongji University.

His research interests include noise and torque ripple of PMSM, vibration and noise of electrical vehicles, and vehicle system dynamics.



Xudong Wu was born in Jiangsu, China, in 1983. He received the PhD degree in Vehicle Engineering from Tongji University in 2011 and then continued his research in the post-doctorate station of Tongji University.

He is the author of over 10 journal / international conference papers and most of them are indexed by EI, SCI and / or ISTP. Since 2013, he has been an Assistant Professor in Vehicle Engineering, School of Automotive Studies, Tongji University. His current research interests include vehicle system dynamics and automotive noise, vibration and harshness issues.